NUMERICAL EXPERIMENTS WITH A ONE-DIMENSIONAL HIGHER ORDER TURBULENCE MODEL: SIMULATION OF THE WANGARA DAY 33 CASE

CHAING CHEN and WILLIAM R. COTTON

Department of Atmospheric Science, Colorado State University, Fort Collins, CO 80523, U.S.A.

(Received in final form 11 January, 1983)

Abstract. A one-dimensional stratocumulus model is developed and incorporated into a cloud/mesoscale model to simulate the evolution of the marine stratocumulus-capped mixed layer.

This paper describes the formulation of the higher-order turbulence model. In a companion paper (Chen and Cotton, 1983), the formulation of the atmospheric radiation model, the partial condensation and the cloud fractional parameterization are described.

The second-order moments of this model are partially diagnosed. In order to close the system, the parameterization for the third-order moments given by Zeman and Lumley (1976) is adopted and is generalized to include total water and cloud water. A new scheme to parameterize the skewness terms is proposed in order to satisfy the enforced realizability. Those skewness terms are used to close the third-order moments.

In this paper, experiments are carried out to test the turbulence model by using the Wangara Day 33 data, which represents a 'dry' case study. Sensitivity experiments using the turbulence length scale parameterizations formulated by André *et al.* (1978) and Sun and Ogura (1980) are reformed and are compared.

1. Introduction

In recent years, Oliver *et al.* (1978), Moeng (1979) and Deardorff (1980) have discussed the simulation of the evolution of the stratocumulus-capped mixed layer. In an attempt to simulate this layer, a one-dimensional stratocumulus model has been developed at Colorado State University (CSU). This model consists of four major parts: (1) a one-dimensional (1D) option of the CSU Cloud/Mesoscale Model (Tripoli and Cotton, 1982), (2) a partially-diagnostic higher-order turbulence model, (3) an atmospheric radiation model with both short- and long-wave radiative transfer through a clear, fully cloudy or partly cloudy atmosphere, and (4) a partial condensation scheme and cloud fractional parameterization. In this paper, the formulation of the turbulence model will be described. The turbulence parameterization will then be tested against the Wangara Day 33 data. In a companion paper (Chen and Cotton, 1983), the atmospheric radiation model and the partial condensation-cloud fractional scheme are introduced. Numerical experiments are then carried out to examine the evolution of the stratocumulus-capped mixed layer.

The current version of the CSU cloud/mesoscale model is a nonhydrostatic, multi-dimensional model which is evolved from a pure cloud model (Cotton and Tripoli, 1978). This cloud/mesoscale model utilizes a pre-processor (PP1) package which has been developed at NCAR over several years. Because of the convenience of this PP1 software, the cloud/mesoscale model can have different versions for various purposes.

Boundary-Layer Meteorology **25** (1983) 375–404. 0006–8314/83/0254–0375$04.50.

The stratocumulus model is just a special one-dimensional version of the 'core' cloud/mesoscale model.

The second-order moment equations were originally derived by Manton and Cotton (1977, hereafter referred to as MC). Banta and Cotton (1979, hereafter referred to as BC) modified MC's equations and obtained a set of partially-diagnostic equations for second-order moments. BC's parameterization is further extended in this paper by including the prognostic equations on all covariances with vertical velocity.

The parameterization (Zeman and Lumley, 1976: hereafter referred to as ZL) for the third-order moments is followed and is also generalized to include the total water ($\bar{r}$) and cloud water ($\bar{r}_c$). A similar approach can be found in Sun and Ogura (1980, hereafter referred to as SO) who extended ZL's scheme by adding total water.

In order to prevent computational instability, some limitations are applied to the second- and third-order moments. A simple realization constraint is applied to the second-order moments, i.e., the variances are always positive definite and the covariances are constrained by the products of variances (for example: $\overline{\alpha''^2}$, $\overline{\beta''^2} \geq 0$, $\overline{\alpha'' \beta''} \leq \sqrt{\overline{\alpha''^2}\,\overline{\beta''^2}}$, where α'' and β'' are any turbulence variables). The third-order moments are constrained by the so-called clipping approximation (André, 1976).

Neither ZL nor SO diagnoses the skewness terms ($\overline{\theta_{il}''^3}$, $\overline{r''^3}$, $\overline{\theta_{il}''^2 r''}$, $\overline{\theta_{il}'' r''^2}$) explicitly, where θ_{il} is the ice-liquid water potential temperature (see Tripoli and Cotton, 1981). Instead they are implicitly incorporated in the following terms: $\overline{w'' \theta_{il}''^2}$, $\overline{w'' r''^2}$, $\overline{w'' \theta_{il}'' r''}$. This introduces the risk that the sknewness terms no longer satisfy the enforced realizability constraint. Therefore, a new scheme to parameterize the skewness terms is developed.

Unlike Deardorff's (1980) model, this 1D stratocumulus model does not have a surface energy budget parameterization from which the surface heat flux and the surface moisture flux can be obtained. Therefore, the surface heat and moisture fluxes used in this 1D boundary layer model are obtained from the numerical experiments reported by André *et al.* (1978; hereafter referred to as AND). Using similarity theory, the surface temperature and moisture can then be calculated from the surface heat flux and moisture flux. Other surface turbulence variables can then be diagnosed using the equations derived by MC.

In this paper, the time integration starts at 0900 local time of Day 33, Wangara. At that time all the turbulence variables are set to be zero. The large-scale E-W geostrophic wind $\bar{u}_g$ varies from 5.5 m s^{-1} near the surface to -2.6 m s^{-1} at 1 km and to -1.2 m s^{-1} at 2 km. The N–S geostrophic wind $\bar{v}_g$ is assumed to be zero all the time.

Two case studies are carried out to compare solutions obtained using AND's and SO's estimates of the turbulence length scale. The results demonstrate that both second- and third-order moments are sensitive to the formulation of the turbulence time scale. Blackadar's approach to the turbulence time scale has been used for nearly twenty years. It is quite appropriate to apply to the unstable mixed layer where the source of convective instability is the heat flux from the earth's surface. However, it may not be appropriate to use in the cloudy layer, where the source of convective instability is long-wave radiation cooling near the cloud top.

2. The CSU Cloud/Mesoscale Model

The CSU Cloud/Mesoscale model has been developed to understand the dynamics of cumulus convection. The first generation of the current model is described by Cotton and Tripoli (1978). In this version, potential temperature is used as a prognostic thermodynamic variable. In the newest version, ice-liquid water potential temperature (θ_{il}) is used (see Tripoli and Cotton, 1982). θ_{il} is a conservative quantity for ice-saturated adiabatic ascent as well as conventional moist adiabatic ascent. θ_{il} is equivalent to θ when ice and liquid water are not present. Tripoli and Cotton (1981) derived a semi-empirical equation for θ, which is a function of θ_{il} and all water phase changes. This semi-empirical equation has proved to be comparably accurate to commonly used irreversible forms of the first law of thermodynamics. The advantages of using θ_{il} are as follows:

(1) cloud water can be diagnosed by 'a partial condensation' scheme.

(2) the thermodynamics can be simplified when the ice phase is introduced into the model.

(3) the model is more amenable to the introduction of higher-order turbulence assumptions.

Although experiments presented in this paper are for a dry case, the governing equations for the first-order moments for a horizontally-homogeneous, non-precipitating cloud system can be summarized as follows:

$$\frac{\partial \bar{u}}{\partial t} = f\bar{v} - f\bar{v}_g + \frac{\partial}{\partial z}(-\overline{u'' w''}),$$

$$\frac{\partial \bar{v}}{\partial t} = -f\bar{u} + f\bar{u}_g + \frac{\partial}{\partial z}(-\overline{v'' w''}),$$

$$\frac{\partial \bar{\theta}_{il}}{\partial t} = -\frac{\partial}{\partial z}(\overline{w'' \theta_{il}''})$$

$$\frac{\partial \bar{r}}{\partial t} = -\frac{\partial}{\partial z}(\overline{w'' r''}), \tag{1}$$

where the mean wind in the x, y, and z directions are $\bar{u}$, $\bar{v}$, and $\bar{w}$, respectively. $\bar{u}_g$ and $\bar{v}_g$ are geostrophic winds, and the coriolis parameter f at Hay, Australia is $-8.26 \times 10^{-5}\ \mathrm{s}^{-1}$. The total water mixing ratio is represented by $\bar{r}$. The turbulence fluctuations from $\bar{u}$, $\bar{v}$, $\bar{w}$, $\bar{\theta}_{il}$, and $\bar{r}$ are u'', v'', w'', θ_{il}'', and r'', respectively. Since the emphasis in this paper is on 'dry' simulations, the 'partial condensation' scheme for cloud water will not be presented here and θ_{il} reduced to the standard definition of dry air potential temperature θ.

3. The Higher-Order Turbulence Model

This stratocumulus model has prognostic equations on $\overline{u''^2}$ + $\overline{v''^2}$, $\overline{w''^2}$, $\overline{\theta_{il}''^2}$, $\overline{r''^2}$, $\overline{\theta_{il}'' r''}$, $\overline{u'' w''}$, $\overline{v'' w''}$, $\overline{w'' \theta_{il}''}$, $\overline{w'' r''}$ and has diagnostic equations for $\overline{u'' v''}$, $\overline{u'' \theta_{il}''}$, $\overline{u'' r''}$, $\overline{v'' r''}$.

In order to close the second-order moment equations, the parameterization for the third-order moments formulated by ZL is utilized. However, ZL's scheme is generalized to include total water and cloud water. In order to complete the closure model, a turbulence time scale must be defined.

Various schemes to parameterize the turbulence time scale can be found in the literature. ZL employed a prognostic equation for the dissipation of turbulence kinetic energy. The turbulence time scale is then a function of the rate of turbulence dissipation. Oliver *et al.* (1978), on the other hand, predict a turbulence length scale instead of time scale. Moeng (1979), SO and AND simplify the problem by adopting a diagnostic equation for the length scale following procedures outlined by Blackadar (1962).

3.1. Second-order moment equations

(a) The generalized prognostic equation for the Reynolds Stress tensor for a horizontally-homogeneous cloud field can be written as

$$\frac{\partial}{\partial t}\overline{u_i'' u_k''} + \bar{w}\frac{\partial}{\partial z}\overline{u_i'' u_k''} = \underbrace{-\left(\overline{u_i'' w''}\frac{\partial}{\partial z}\bar{u}_k + \overline{u_k'' w''}\frac{\partial}{\partial z}\bar{u}_i\right)}_{\text{A}} \underbrace{-\frac{\partial}{\partial z}(\overline{u_i'' u_k'' w''})}_{\text{B}}$$

$$\underbrace{-\frac{g}{\rho_0}(\overline{\rho'' u_i''}\,\delta_{3k} + \overline{\rho'' u_k''}\,\delta_{3i})}_{\text{C}} \underbrace{-\frac{1}{\rho_0}\left(\overline{u_i''\frac{\partial p''}{\partial x_k}} + \overline{u_k''\frac{\partial p''}{\partial x_i}}\right)}_{\text{D}}$$

$$\underbrace{-\tfrac{2}{3}\bar{\varepsilon}\delta_{ik}}_{\text{E}} \qquad (2)$$

where (u_i'', i = 1–3) represent (u'', v'', w''), ρ'' and p'' represent the fluctuations of density and pressure, respectively, and ρ_0 is the reference state air density. The various terms on the right-hand side (RHS) of Equation (2) are described as follows:

(i) Term A represents the mechanical production of $\overline{u_i'' u_k''}$ by the vertical shear of $\bar{u}_i$ and $\bar{u}_k$.

(ii) Term B can be described as the vertical transport of Reynolds stress by eddies. These eddies are usually driven by buoyancy in the heated planetary boundary layer (PBL).

(iii) Term C is the production of $\overline{u_i'' u_k''}$ by buoyancy, which is the major and dominant term in the Reynolds stress equation for an unstable PBL.

(iv) Term D is the change of $\overline{u_i'' u_k''}$ due to the pressure – velocity correlations. Term D

can also be represented by

$$-\frac{1}{\rho_0}\left(u_i''\,\overline{\frac{\partial p''}{\partial x_k}}+u_k''\,\overline{\frac{\partial p''}{\partial x_i}}\right)=-\frac{1}{\rho_0}\left(\overline{\frac{\partial p''}{\partial x_i}}\,u_k''+\overline{\frac{\partial p''}{\partial x_k}}\,u_i''-\tfrac{2}{3}\delta_{ik}\,\frac{\partial}{\partial x_j}\,\overline{p''u_j''}\right)$$

$$-\tfrac{2}{3}\delta_{ik}\,\frac{1}{\rho_0}\,\frac{\partial}{\partial x_j}\,\overline{p''u_j''}\,. \tag{3}$$

The first term on the RHS of Equation (3) represents the return to isotropy, i.e., the pressure fluctuation redistributes the energy between $\overline{u''^2}$, $\overline{v''^2}$, and $\overline{w''^2}$. The second term represents the vertical transport by the pressure fluctuation.

(v) The last term E represents the destruction of $\overline{u_i''u_k''}$ due to molecular dissipation.

According to Equation (2), the complete set of Reynolds stress equations can be written as follows:

$$\frac{\partial}{\partial t}\,\bar{e}=-\bar{w}\,\frac{\partial}{\partial z}\,\bar{e}-2\overline{u_i''w''}\,\frac{\partial}{\partial z}\,\bar{u}_i-\frac{\partial}{\partial z}\left(\overline{u_i''u_i''w''}+\frac{4}{3}\,\frac{1}{\rho_0}\,\overline{p''w''}\right)$$

$$-\pi_{ii}-\tfrac{4}{3}\bar{\varepsilon}\,;\qquad i=1-2 \tag{4}$$

where $e=\overline{u''^2}+\overline{v''^2}$ and

$$\frac{\partial}{\partial t}\,\overline{w''^2}=-\bar{w}\,\frac{\partial}{\partial z}\,\overline{w''^2}-2\overline{w''^2}\,\frac{\partial}{\partial z}\,\bar{w}-\frac{2g}{\rho_0}\,\overline{\rho''w''}$$

$$-\frac{\partial}{\partial z}\left(\overline{w''^2}+\frac{2}{3}\,\frac{1}{\rho_0}\,\overline{p''w''}\right)-\pi_{33}-\tfrac{2}{3}\bar{\varepsilon}\,, \tag{5}$$

and

$$\frac{\partial}{\partial t}\,\overline{u_i''w''}=-\bar{w}\,\frac{\partial}{\partial z}\,\overline{u_i''w''}-2\overline{u_i''w''}\,\frac{\partial}{\partial z}\,\bar{w}-\overline{w''^2}\,\frac{\partial}{\partial z}\,\bar{u}_i-\frac{\partial}{\partial z}\,\overline{u_i''w''^2}$$

$$-\frac{g}{\rho_0}\,\overline{\rho''u_i''}-\pi_{i3}\,;\qquad i=1-2\,. \tag{6}$$

The isotropy term

$$\pi_{ik}=-\frac{1}{\rho_0}\left(\overline{\frac{\partial p''}{\partial x_i}}\,u_k''+\overline{\frac{\partial p''}{\partial x_k}}\,u_i''-\tfrac{2}{3}\delta_{ik}\,\frac{\partial}{\partial x_j}\,\overline{p''u_j''}\right)$$

which can be parameterized following ZL (1976) and is defined by

$$\pi_{ik} = \frac{C_1}{\tau} b_{ik} q^2 - 3/10 R_1 (\overline{u_i'' \theta_{il}''} \delta_{3k} + \overline{u_k'' \theta_{il}''} \delta_{3i} - \tfrac{2}{3} \overline{w'' \theta_{il}''} \delta_{ik}) - 3/10 R_2 (\overline{u_i'' r''} \delta_{3k} + \overline{u_k'' r''} \delta_{3i} - \tfrac{2}{3} \overline{w'' r''} \delta_{ik}) - 3/10 R_3 (\overline{u_i'' r_c''} \delta_{3k} + \overline{u_k'' r_c''} \delta_{3i} - \tfrac{2}{3} \overline{w'' r_c''} \delta_{ik}) \tag{7}$$

where $b_{ik} = \overline{u_i'' u_k''}/q^2 - \frac{1}{3}\delta_{ik}$; $C_1 = 1$, and the turbulent time scale is represented by τ. The coefficients R_1, R_2, and R_3 are related to the buoyancy effect, which is introduced later. The turbulence energy q^2 is given by $q^2 = \overline{u_j'' u_j''} = \bar{e} + \overline{w''^2}$. If we assume $(\partial/\partial t)\overline{u'' v''} = 0$, and no vertical divergence of the triple term, then the diagnostic equation for $\overline{u'' v''}$ can be written as

$$\overline{u'' v''} \left(\frac{\partial \bar{w}}{\partial z} + \frac{C_1}{\tau} \right) = - \overline{u'' w''} \frac{\partial}{\partial z} \bar{v} - \overline{u'' w''} \frac{\partial}{\partial z} \bar{u} . \tag{8}$$

For a buoyancy-driven, well-mixed boundary layer, the steady-state approximation for $\overline{u'' v''}$ may be appropriate.

(b) The remainder of the second-order moment equations used in the model can be summarized as follows:

$$\frac{\partial}{\partial t} \overline{\theta_{il}''^2} = - \bar{w} \frac{\partial}{\partial z} \overline{\theta_{il}^2} - 2\overline{w'' \theta_{il}''} \frac{\partial}{\partial z} \bar{\theta}_{il} - \frac{\partial}{\partial z} \overline{w'' \theta_{il}''^2} - 2\bar{\varepsilon}_0 \tag{9}$$

$$\frac{\partial}{\partial t} \overline{r''^2} = - \bar{w} \frac{\partial}{\partial z} \overline{r''^2} - 2\overline{w'' r''} \frac{\partial}{\partial z} \bar{r} - \frac{\partial}{\partial z} \overline{w'' r''^2} - 2\bar{\varepsilon}_r \tag{10}$$

$$\frac{\partial}{\partial t} \overline{\theta_{il}'' r''} = - \bar{w} \frac{\partial}{\partial z} \overline{\theta_{il}'' r''} - \overline{w'' \theta_{il}''} \frac{\partial}{\partial z} \bar{r} - \overline{w'' r''} \frac{\partial}{\partial z} \bar{\theta}_{il} - \frac{\partial}{\partial z} \overline{w'' \theta_{il}'' r''} - 2\bar{\varepsilon}_{\theta r} \tag{11}$$

$$\frac{\partial}{\partial t} \overline{w'' \theta_{il}''} = - \bar{w} \frac{\partial}{\partial z} \overline{w'' \theta_{il}''} - \overline{w'' \theta_{il}''} \frac{\partial}{\partial z} \bar{w} - \overline{w''^2} \frac{\partial}{\partial z} \bar{\theta}_{il} - \frac{\partial}{\partial z} \overline{w''^2 \theta_{il}''} - \frac{g}{\rho_0} \overline{\rho'' \theta_{il}''} - \pi_{30} \tag{12}$$

$$\frac{\partial}{\partial t}\overline{w'' r''} = -\bar{w}\frac{\partial}{\partial z}\overline{w'' r''} - \overline{w'' r''}\frac{\partial}{\partial z}\bar{w} - \overline{w''^2}\frac{\partial}{\partial z}\bar{r} - \frac{\partial}{\partial z}\overline{w''^2 r''}$$

$$-\frac{g}{\rho_0}\overline{\rho'' r''} - \pi_{3r} \tag{13}$$

where

$$\pi_{3\theta} = -\frac{1}{\rho_0}\overline{\frac{\partial p''}{\partial z}\theta_{il}''}, \qquad \pi_{3r} = -\frac{1}{\rho_0}\overline{\frac{\partial p''}{\partial z} r''}, \tag{14}$$

which represent the pressure gradient – θ_{il} and pressure gradient – r correlation, respectively, and can be approximated following AND as

$$\pi_{3\theta} = \frac{C_\theta}{\tau}\overline{w'' \theta_{il}''} - \tfrac{1}{3}(R_1\overline{\theta_{il}''^2} + R_2\overline{\theta_{il}'' r''} + R_3\overline{\theta_{il}'' r_c''}) \tag{15}$$

$$\pi_{3r} = \frac{C_\theta}{\tau}\overline{w'' r''} - \tfrac{1}{3}(R_1\overline{\theta_{il}'' r''} + R_2\overline{r''^2} + R_3\overline{r'' r_c''}) \tag{16}$$

where $C_\theta = 2.17$.

The covariance of θ_{il}'' and r'' with respect to u'' and v'' can be estimated by the same assumptions used to obtain $\overline{u'' v''}$. Thus, the diagnostic equations for $\overline{u'' \theta_{il}''}$, $\overline{v'' \theta_{il}''}$, $\overline{u'' r''}$, and $\overline{v'' r''}$ can be written as

$$\overline{u_i'' \theta_{il}''}(C_\theta/\tau) = -\overline{u_i'' w''}\frac{\partial}{\partial z}\bar{\theta}_{il} - \overline{w'' \theta_{il}''}\frac{\partial}{\partial z}\bar{u}_i; \qquad i = 1-2 \tag{17}$$

$$\overline{u_i'' r''}(C_\theta/\tau) = -\overline{u_i'' w''}\frac{\partial}{\partial z}\bar{r} - \overline{w'' r''}\frac{\partial}{\partial z}\bar{u}_i; \qquad i = 1-2 \tag{18}$$

(c) The covariances with density fluctuations can be further derived as follows:

From MC, the total density fluctuation equation including condensate can be written as:

$$\frac{\rho''}{\rho_0} = (1 - R_a/C_{pa})(P''/P_0) - \theta''/\theta_0 - (R_v/R_a - 1)r'' + R_v/R_a(r_l'') \tag{19}$$

where '0' denotes the reference state, r_l'' is the fluctuation of all liquid water mixing ratio. For a non-precipitating system, $r_l'' = r_c''$.

From the definition of θ_{il}, θ can be expressed by

$$\theta'' = \theta_{il}'' + \frac{L_{lv}\theta_0}{c_{pa}T_0} r_l''. \tag{20}$$

Before substituting the above equation into the density perturbation equation, the pressure perturbation (p'') can be assumed to be insignificant for shallow convection and turbulence scales. The final form of the equation can be written as

$$\frac{\rho''}{\rho_0} = -\frac{\theta_{il}''}{\theta_0} - (R_v/R_a - 1)r'' - \left(\frac{L_{lv}}{c_{pa}T_0} - R_v/R_a\right) r_l'' \,. \tag{21}$$

The covariance with density perturbation can then be represented by

$$\frac{-g}{\rho_0}\,\overline{\rho''\,\alpha''} = -R_1\,\overline{\theta_{il}''\,\alpha''} - R_2\,\overline{r''\,\alpha''} - R_3\,\overline{r_l''\,\alpha''} \tag{22}$$

where α'' can be any turbulent fluctuation. Coefficients R_1, R_2, and R_3 are

$$\begin{aligned} R_1 &= -g/\theta_0 \\ R_2 &= -(R_v/R_a - 1)g \\ R_3 &= -(L_{lv}/c_{pa}T_0 - R_v/R_a)g \,. \end{aligned} \tag{23}$$

3.2. The third-order moment equations

ZL's parameterization for third-order moments is adopted and extended to include total water and cloud water. The prognostic equation for the third-order moments can be represented by the following equation:

$$\frac{\partial F_i}{\partial t} = SG_i + SB_i - F_i/\tau_3 - D_i \tag{24}$$

where F_i represents any third-order moment, and SG_i and SB_i are the production of F_i due to turbulence-velocity interaction and buoyancy, respectively. F_i/τ_3 is the return to isotropy due to pressure-velocity interaction. D_i is the viscous term. The turbulence time scale for the third-order moments is τ_3.

The basic assumption that ZL utilize to close the third-order moment terms is that the local rate of change of the third-order moment is approximately zero, i.e.,

$$\frac{\partial F_i}{\partial t} \simeq 0 \,.$$

Thus a diagnostic equation for F_i can be obtained from Equation (24).

In the buoyance-driven boundary layer, the vertical transport of second-order quantities by eddies is our major concern. Therefore, the parameterization of third-order moments includes the terms $\overline{w''r''^2}$, $\overline{w''\theta_{il}''^2}$, $\overline{w''\theta_{il}''r''}$, $\overline{w''^2r''}$, $\overline{w''^2\theta_{il}''}$, $\overline{w''^3}$, $\overline{u''^2w''}$, $\overline{v''^2w''}$, $\overline{u''w''^2}$, $\overline{v''w''^2}$, $\overline{\theta_{il}''^3}$, $\overline{\theta_{il}''^2r''}$, $\overline{\theta_{il}''r''^2}$, $\overline{r''^3}$.

The terms in the RHS of Equation (24) can be summarized as follows:

$$SG = \begin{bmatrix} \overline{w''r''^2} \\ \overline{w''\theta_{il}''^2} \\ \overline{w''\theta_{il}''r''} \\ \\ \overline{w''^2r''} \\ \overline{w''^2\theta_{il}''} \\ \overline{w''^3} \\ \overline{u''^2w''} \\ \overline{v''^2w''} \\ \overline{u''w''^2} \\ \overline{v''w''^2} \\ \theta_{il}''^3 \\ \overline{\theta_{il}''^2r''} \\ \\ \overline{\theta_{il}''r''^2} \\ \\ \overline{r''^3} \end{bmatrix} = \begin{bmatrix} -\overline{w''^2}\,\frac{\partial}{\partial z}\,\overline{r''^2} - 2\overline{w''r''}\,\frac{\partial}{\partial z}\,\overline{w''r''} \\ -\overline{w''^2}\,\frac{\partial}{\partial z}\,\overline{\theta_{il}''^2} - 2\overline{w''\theta_{il}''}\,\frac{\partial}{\partial z}\,\overline{w''\theta_{il}''} \\ -\overline{w''^2}\,\frac{\partial}{\partial z}\,\overline{\theta_{il}''r''} - w''\theta_{il}''\,\frac{\partial}{\partial z}\,\overline{w''r''} \\ -\overline{w''r''}\,\frac{\partial}{\partial z}\,\overline{w''\theta_{il}''} \\ -2\overline{w''^2}\,\frac{\partial}{\partial z}\,\overline{w''r''} - \overline{w''r''}\,\frac{\partial}{\partial z}\,\overline{w''^2} \\ -2\overline{w''^2}\,\frac{\partial}{\partial z}\,\overline{w''\theta_{il}''} - \overline{w''\theta_{il}''}\,\frac{\partial}{\partial z}\,\overline{w''^2} \\ -3\overline{w''^2}\,\frac{\partial}{\partial z}\,\overline{w''^2} \\ -\overline{w''^2}\,\frac{\partial}{\partial z}\,\overline{u''^2} - 2\overline{u''w''}\,\frac{\partial}{\partial z}\,\overline{u''w''} \\ -\overline{w''^2}\,\frac{\partial}{\partial z}\,\overline{v''^2} - 2\overline{v''w''}\,\frac{\partial}{\partial z}\,\overline{v''w''} \\ -\overline{u''w''}\,\frac{\partial}{\partial z}\,\overline{w''^2} - 2\overline{w''^2}\,\frac{\partial}{\partial z}\,\overline{u''w''} \\ -\overline{v''w''}\,\frac{\partial}{\partial z}\,\overline{w''^2} - 2\overline{w''^2}\,\frac{\partial}{\partial z}\,\overline{v''w''} \\ -3\overline{w''\theta_{il}''}\,\frac{\partial}{\partial z}\,\overline{\theta_{il}''^2} - 3\overline{w''\theta''^2}\,\frac{\partial}{\partial z}\,\overline{\theta}_{il} \\ -\overline{w''r''}\,\frac{\partial}{\partial z}\,\overline{\theta_{il}''^2} - 2\overline{w''\theta_{il}''}\,\frac{\partial}{\partial z}\,\overline{\theta_{il}''r''} \\ -\overline{w''\theta_{il}''^2}\,\frac{\partial}{\partial z}\,\bar{r} - 2\overline{w''\theta_{il}''r''}\,\frac{\partial}{\partial z}\,\overline{\theta}_{il} \\ -\overline{w''\theta_{il}''}\,\frac{\partial}{\partial z}\,\overline{r''^2} - 2\overline{w''r''}\,\frac{\partial}{\partial z}\,\overline{\theta_{il}''r''} \\ -\overline{w''r''^2}\,\frac{\partial}{\partial z}\,\overline{\theta}_{il} - 2\overline{w''\theta_{il}''r''}\,\frac{\partial}{\partial z}\,\bar{r} \\ -3\overline{w''r''}\,\frac{\partial}{\partial z}\,\overline{r''^2} - 3\overline{w''r''^2}\,\frac{\partial}{\partial z}\,\bar{r} \end{bmatrix} \tag{25}$$

$$SB = \begin{bmatrix} \overline{w'' r''^2} \\ \overline{w'' \theta_{il}''^2} \\ \overline{w'' \theta_{il}'' r''} \\ \overline{w''^2 r''} \\ \overline{w''^2 \theta_{il}''} \\ \overline{w''^3} \\ \overline{u''^2 w''} \\ \overline{v''^2 w''} \end{bmatrix} = \begin{bmatrix} -R_1 \overline{\theta_{il}'' r''^2} - R_2 \overline{r''^3} - R_3 \overline{r''^2 r_c''} \\ -R_1 \overline{\theta_{il}''^3} - R_2 \overline{\theta_{il}''^2 r''} - R_3 \overline{\theta_{il}''^2 r_c''} \\ -R_1 \overline{\theta_{il}''^2 r''} - R_2 \overline{\theta_{il}'' r''^2} - R_3 \overline{\theta_{il}'' r'' r_c''} \\ -\frac{5}{3}(R_1 \overline{w'' \theta_{il}'' r''} + R_2 \overline{w'' r''^2} + R_3 \overline{w'' r'' r_c''}) \\ -\frac{5}{3}(R_1 \overline{w'' \theta_{il}''^2} + R_2 \overline{w'' \theta_{il}'' r''} + R_3 \overline{w'' \theta_{il}'' r_c''}) \\ -\frac{13}{5}(R_1 \overline{w''^2 \theta_{il}''} + R_2 \overline{w''^2 r''} + R_3 \overline{w''^2 r_c''}) \\ -\frac{1}{5}(R_1 \overline{w''^2 \theta_{il}''} + R_2 \overline{w''^2 r''} + R_3 \overline{w''^2 r_c''}) \\ -\frac{1}{5}(R_1 \overline{w''^2 \theta_{il}''} + R_2 \overline{w''^2 r''} + R_3 \overline{w''^2 r_c''}) \end{bmatrix} \tag{26}$$

$$D = \begin{bmatrix} \overline{w'' r''^2} \\ \overline{w'' \theta_{il}''^2} \\ \overline{w'' \theta_{il}'' r''} \\ \overline{w''^2 r''} \\ \overline{w''^2 \theta_{il}''} \\ \overline{w''^3} \\ \overline{u''^2 w''} \\ \overline{v''^2 w''} \\ \overline{\theta_{il}''^3} \\ \overline{\theta_{il}''^2 r''} \\ \overline{\theta_{il} r''^2} \\ \overline{r''^3} \end{bmatrix} = \begin{bmatrix} \frac{2\mu}{\tau_0} \overline{w'' r''^2} \\ \frac{2\mu}{\tau_0} \overline{w'' \theta_{il}^2} \\ \frac{2\mu}{\tau_0} \overline{w'' \theta_{il}'' r''} \\ \frac{4\mu}{3\tau} \overline{w''^2 r''} \\ \frac{4\mu}{3\tau} \overline{w''^2 \theta_{il}''} \\ \frac{2\mu}{\tau} \overline{q^2 w''} \\ \frac{2\mu}{3\tau} \overline{q^2 w''} \\ \frac{2\mu}{3\tau} \overline{q^2 w''} \\ \frac{2\mu}{\tau_0} \overline{\theta_{il}''^3} \\ \frac{2\mu}{\tau_0} \overline{\theta_{il}''^2 r''} \\ \frac{2\mu}{\tau_0} \overline{\theta_{il}'' r''^2} \\ \frac{2\mu}{\tau_0} \overline{r''^3} \end{bmatrix} \tag{27}$$

The diagnostic equations for $\overline{w'' r''^2}$, $\overline{w'' \theta_{il}''^2}$, $\overline{w'' \theta_{il}'' r''}$, $\overline{w''^2 r''}$, $\overline{w''^2 \theta_{il}''}$, $\overline{w''^3}$, $\overline{u''^2 w''}$, and $\overline{v''^2 w''}$ can be written as follows:

$$\overline{w'' r''^2}\left(\frac{1}{\tau_3}+\frac{2\mu}{\tau_\theta}\right) = -\overline{w''^2}\,\frac{\partial}{\partial z}\,\overline{r''^2} - 2\overline{w'' r''}\,\frac{\partial}{\partial z}\,\overline{w'' r''} - R_1\overline{\theta_{il}'' r''^2} - R_2\overline{r''^3} - R_3\overline{r''^2 r_c''}$$

$$\overline{w'' \theta_{il}''^2}\left(\frac{1}{\tau_3}+\frac{2\mu}{\tau_\theta}\right) = -\overline{w''^2}\,\frac{\partial}{\partial z}\,\overline{\theta_{il}''^2} - 2\overline{w'' \theta_{il}''}\,\frac{\partial}{\partial z}\,\overline{w'' \theta_{il}''} - R_1\overline{\theta_{il}''^3} - R_2\overline{\theta_{il}''^2 r''} - R_3\overline{\theta_{il}''^2 r_c''}$$

$$\overline{w'' \theta_{il}'' r''}\left(\frac{1}{\tau_3}+\frac{2\mu}{\tau_\theta}\right) = -\overline{w''^2}\,\frac{\partial}{\partial z}\,\overline{\theta_{il}'' r''} - \overline{w'' \theta_{il}''}\,\frac{\partial}{\partial z}\,\overline{w'' r''} - \overline{w'' r''}\,\frac{\partial}{\partial z}\,\overline{w'' \theta_{il}''} - R_1\overline{\theta_{il}''^2 r''} - R_2\overline{\theta_{il}'' r''^2} - R_3\overline{\theta_{il}'' r'' r_c''} \tag{28}$$

$$\overline{w''^2 r''}\left(\frac{1}{\tau_3}+\frac{4\mu}{3\tau}\right) = -2\overline{w''^2}\,\frac{\partial}{\partial z}\,\overline{w'' r''} - \overline{w'' r''}\,\frac{\partial}{\partial z}\,\overline{w''^2} - \tfrac{5}{3}(R_1\overline{w'' \theta_{il}'' r''} + R_2\overline{w'' r''^2} + R_3\overline{w'' r'' r_c''})$$

$$\overline{w''^2 \theta_{il}''}\left(\frac{1}{\tau_3}+\frac{4\mu}{3\tau}\right) = -2\overline{w''^2}\,\frac{\partial}{\partial z}\,\overline{w'' \theta_{il}''} - \overline{w'' \theta_{il}''}\,\frac{\partial}{\partial z}\,\overline{w''^2} - \tfrac{5}{3}(R_1\overline{w'' \theta_{il}''^2} + R_2\overline{w'' \theta_{il}'' r''} + R_3\overline{w'' \theta_{il}'' r_c''})$$

$$\begin{aligned}\overline{q^2 w''}\left(\frac{1}{\tau_3}+\frac{4\mu}{3\tau}+\frac{2\mu}{\tau}\right) &= (\overline{u''^2 w''} + \overline{v''^2 w''} + \overline{w''^3})\left(\frac{1}{\tau_3}+\frac{4\mu}{3\tau}+\frac{2\mu}{\tau}\right)\\ &= -\overline{w''^2}\,\frac{\partial}{\partial z}\,\overline{u''^2} - 2\overline{u'' w''}\,\frac{\partial}{\partial z}\,\overline{u'' w''}\\ &\quad - \overline{w''^2}\,\frac{\partial}{\partial z}\,\overline{v''^2} - 2\overline{v'' w''}\,\frac{\partial}{\partial z}\,\overline{v'' w''} - 3\overline{w''^2}\,\frac{\partial}{\partial z}\,\overline{w''^2}\\ &\quad - 3(R_1\overline{w''^2 \theta_{il}''} + R_2\overline{w''^2 r''} + R_3\overline{w''^2 r_c''})\,.\end{aligned}$$

In the convectively-driven boundary layer, $\overline{w''^2}$ is the dominant term. In order to have a reasonable redistribution of energy among $\overline{w''^3}$, $\overline{u''^2 w''}$, and $\overline{v''^2 w''}$, we use a simple approximation that $\overline{w''^3} = \frac{1}{2}\overline{q^2 w''}$

$$\overline{u''^2 w''} = \overline{v''^2 w''} = \tfrac{1}{2}\overline{w''^3}\,.$$

The diagnostic equations for $\overline{u'' w''^2}$, $\overline{v'' w''^2}$ and the skewness terms $\overline{\theta_{il}''^3}$, $\overline{\theta_{il}''^2 r''}$, $\overline{\theta_{il} r''^2}$, $\overline{r''^3}$ are obtained by assuming $SG_i - D_i = 0$.

Therefore

$$\overline{u_i'' w''^2}\left(\frac{1}{\tau_3} + \frac{4\mu}{3\tau}\right) = -\overline{u_i'' w''}\ \frac{\partial}{\partial z}\overline{w''^2} - 2\overline{w''^2}\ \frac{\partial}{\partial z}\overline{u_i'' w''}\,; \qquad i = 1 - 2$$

$$\overline{\theta_{il}''^3} = -\frac{\tau_0}{2\mu}\left(3\overline{w'' \theta_{il}''}\ \frac{\partial}{\partial z}\overline{\theta_{il}''^2} + 3\overline{w'' \theta_{il}''^2}\ \frac{\partial}{\partial z}\overline{\theta_{il}}\right)$$

$$\overline{\theta_{il}''^2 r''} = -\frac{\tau_0}{2\mu}\left(\overline{w'' r''}\ \frac{\partial}{\partial z}\overline{\theta_{il}''^2} + 2\overline{w'' \theta_{il}''}\ \frac{\partial}{\partial z}\overline{\theta_{il}'' r''}\right.$$
$$\left. + \overline{w'' \theta_{il}''^2}\ \frac{\partial}{\partial z}\bar{r} + 2\overline{w'' \theta_{il}'' r''}\ \frac{\partial}{\partial z}\overline{\theta_{il}}\right)$$

$$\overline{\theta_{il}'' r''^2} = -\frac{\tau_0}{2\mu}\left(\overline{w'' \theta_{il}''}\ \frac{\partial}{\partial z}\overline{r''^2} + 2\overline{w'' r''}\ \frac{\partial}{\partial z}\overline{\theta_{il}'' r''}\right.$$
$$\left. + \overline{w'' r''^2}\ \frac{\partial}{\partial z}\overline{\theta_{il}} + 2\overline{w'' \theta_{il}'' r''}\ \frac{\partial}{\partial z}\bar{r}\right)$$

$$\overline{r''^3} = -\frac{\tau_0}{2\mu}\left(3\overline{w'' r''}\ \frac{\partial}{\partial z}\overline{r''^2} + 3\overline{w'' r''^2}\ \frac{\partial}{\partial z}\bar{r}\right). \tag{29}$$

Both ZL and SO substitute the skewness terms into Equation (28) and solve for $\overline{w'' \theta_{il}''^2}$, $\overline{w'' r''^2}$ and $\overline{w'' \theta_{il}'' r''}$ directly. However, in their case some parameters must be added in order to obtain positive $\overline{w'' \theta_{il}''^2}$ near the surface. We also find that the solution to the skewness terms may not always satisfy the conditions required of enforced realizability.

A new diagnostic scheme for the skewness terms is introduced as follows. From Equation (28), the first approximation of $\overline{w'' \theta_{il}''^2}$, $\overline{w'' r''^2}$, and $\overline{w'' \theta_{il}'' r''}$ can be written as

$$\overline{w'' \theta_{il}''^2}(A_1) = B_1 - R_1 \overline{\theta_{il}''^3}$$
$$\overline{w'' \theta_{il}'' r''}(A_1) = C_1 - R_1 \overline{\theta_{il}''^2 r''}$$
$$\overline{w'' r''^2}(A_1) = D_1 - R_1 \overline{\theta_{il}'' r''^2} \tag{30}$$

where

$$A_1 = \frac{1}{\tau_3} + \frac{2\mu}{\tau_0}$$

$$B_1 = -\overline{w''^2}\ \frac{\partial}{\partial z}\overline{\theta_{il}''^2} - 2\overline{w'' \theta_{il}''}\ \frac{\partial}{\partial z}\overline{w'' \theta_{il}''}$$

$$C_1 = -\overline{w''^2}\,\frac{\partial}{\partial z}\,\overline{\theta_{il}'' r''} - \overline{w'' \theta_{il}''}\,\frac{\partial}{\partial z}\,\overline{w'' r''} - \overline{w'' r''}\,\frac{\partial}{\partial z}\,\overline{w'' \theta_{il}''}$$

$$D_1 = -\overline{w''^2}\,\frac{\partial}{\partial z}\,\overline{r''^2} - 2\overline{w'' r''}\,\frac{\partial}{\partial z}\,\overline{w'' r''}\,.$$

Substitution of Equation (30) into Equation (29) results in

$$\overline{\theta_{il}''^3}\left(1 - \frac{3\tau_0}{2\mu}\,\frac{R_1}{A_1}\,\frac{\partial\bar{\theta}_{il}}{\partial z}\right) = -\frac{3\tau_0}{2\mu}\left(\overline{w'' \theta_{il}''}\,\frac{\partial}{\partial z}\,\overline{\theta_{il}''^2} + \frac{B_1}{A_1}\,\frac{\partial\bar{\theta}_{il}}{\partial z}\right)$$

$$\overline{\theta_{il}''^2 r''}\left(1 - \frac{\tau_0 R_1}{\mu A_1}\,\frac{\partial\bar{\theta}_{il}}{\partial z}\right) = -\frac{\tau_0}{2\mu}\left(\overline{w'' r''}\,\frac{\partial}{\partial z}\,\overline{\theta_{il}''^2} + 2\overline{w'' \theta_{il}}\,\frac{\partial}{\partial z}\,\overline{\theta_{il}'' r''}\right)$$

$$-\frac{\tau_0}{2\mu}\,\frac{\partial\bar{r}}{\partial z}\left(\frac{B_1}{A_1} - \frac{R_1}{A_1}\,\overline{\theta_{il}''^3}\right) - \frac{\tau_0}{\mu}\,\frac{C_1}{A_1}\,\frac{\partial\bar{\theta}_{il}}{\partial z}$$

$$\overline{\theta_{il}'' r''^2}\left(1 - \frac{\tau_0}{2\mu}\,\frac{R_1}{A_1}\,\frac{\partial\bar{\theta}_{il}}{\partial z}\right) = -\frac{\tau_0}{2\mu}\left(\overline{w'' \theta_{il}''}\,\frac{\partial}{\partial z}\,\overline{r''^2} + 2\overline{w'' r''}\,\frac{\partial}{\partial z}\,\overline{\theta_{il}'' r''}\right)$$

$$-\frac{\tau_0}{2\mu}\,\frac{D_1}{A_1}\,\frac{\partial\bar{\theta}_{il}}{\partial z} - \frac{\tau_0}{\mu}\,\frac{C_1}{A_1}\,\frac{\partial\bar{r}}{\partial z} + \frac{\tau_0}{\mu}\,\frac{R_1}{A_1}\,\frac{\partial\bar{r}}{\partial z}\,\overline{\theta_{il}''^2 r''}$$

$$\overline{r''^3} = -\frac{3\tau_0}{2\mu}\,\overline{w'' r''}\,\frac{\partial}{\partial z}\,\overline{r''^2} - \frac{3\tau_0}{2\mu}\,\frac{\partial\bar{r}}{\partial z}\left(\frac{D_1}{A_1} - \frac{R_1}{A_1}\,\overline{\theta_{il}'' r''^2}\right). \tag{31}$$

All of the skewness terms are enforced by realizability before the rest of the triple correlations are computed by Equation (28). In Equation (28), the triple correlations with cloud water fluctuations can be parameterized as

$$\overline{\alpha'' \beta'' r_c''} = (a_2 \overline{\alpha'' \beta'' r''} - b_2 \overline{\alpha'' \beta'' \theta_{il}''})H \tag{32}$$

where α'' and β'' can be any turbulent variable, H is the cloud fractional coverage and a_2, b_2 are coefficients. The derivation and the determination of H, a_2, b_2 are given in Chen and Cotton (1983).

3.3. The parameterization of dissipation and the turbulence time scale

As mentioned before, $\bar{\varepsilon}$, $\bar{\varepsilon}_0$, $\bar{\varepsilon}_r$, and $\bar{\varepsilon}_{0r}$ represent the mean rates of turbulent energy dissipation and destruction of $\theta_{il}''^2$, r''^2, and $\overline{\theta_{il}'' r''}$ respectively. Various ways can be found in the literature for parameterizing the dissipation and destruction terms. For example, ZL use prognostic equations, while AND and SO diagnose those terms. Both AND and SO approach the above problems by adopting Blackadar's (1962) length scale for an unstable PBL. The advantage of using Blackadar's length scale is its simplicity.

In this approach, the mixing length near the surface is proportional to kz, where k is Von-Karman's constant. This mixing length can be derived from similarity theory. In the well-mixed layer, Blackadar's length scale converges to a constant mixing length of about 50–60 m. A disadvantage of Blackadar's length scale is that it may not be appropriate for use in the unstable cloud layer. This can be explained as follows. The release of latent heat due to condensation or the convective instability created by cloud-top radiation cooling and cloud-base radiation warming may be accompanied by the production of turbulence kinetic energy (TKE). Usually, the dissipation of TKE should respond very quickly to the production of TKE. However, for deep cloud layers where Blackadar's length scale becomes asymptotic, this formulation does not respond correctly. In a companion paper (Chen and Cotton, 1983), a modification to Blackadar's length scale in the cloud layer is described.

In the following sections, we shall compare numerical experiments using two formulations of the length scale based on SO and AND. Table I summarizes the experiments, which are labelled SO and AND. The turbulence length scale l is determined by the minimum of l_B and l_D for the AND case and by the inverse of $(1/l_B) + (1/l_D)$ for the SO case. Blackadar's length scale is l_B, which is the mixing length of a well-mixed layer. The quantity l_0 is also defined in slightly different ways. In SO's case, l_0 is a function of S_l, which is height-dependent. Therefore, SO's l_0 can be smaller near the surface. The coefficient C_1 shown in the dissipation ($\bar{\varepsilon}$) is given as

$$C_1 = 1./15 \text{ (SO)}$$

$$C_1 = 0.102 \text{ (AND)}. \tag{32}$$

André *et al.* (1978) define C_1 as $C_1 = 0.019 + 0.051\, l/l_B$. The ratio (l/l_B) is always small near the inversion, which depends on the strength of the inversion. This ratio is introduced in order to compensate for stability effects. However, the results of sensitivity experiments suggest that the use of this ratio may not be appropriate, especially for a model using a ZL-type closure for the third-order moments. Brost (personal communication) indicates that ZL's scheme is sensitive to the turbulence time scale.

The introduction of l/l_B may lead to a larger turbulence time scale, thus ZL's scheme will not function properly.

The length scale for the stable stratified layer is given by

$$l_D = 0.75\left[\frac{q^2}{2}\Big/\left(-R_1\,\frac{\partial}{\partial z}\,\overline{\theta_{il}}\right)\right]^{1/2} \qquad \text{(AND)}$$

$$l_D = \left[2q^2\Big/\left(-R_1\,\frac{\partial}{\partial z}\,\overline{\theta_{il}}\right)\right]^{1/2}. \qquad \text{(SO)} \tag{33}$$

Although the coefficient of the above two types of parameterization is different, both l_D's are functions of atmospheric stability. The Brunt-Vaisalla frequency can be written as $[-R_1(\partial/\partial z)\overline{\theta_{il}}]^{1/2}$. The larger frequency implies larger dissipation, i.e., smaller mixing length.

TABLE I

Sensitivity experiment for SO and AND cases

Case	$\bar{\varepsilon}$	l	l_B	l_0	C_1	S_l	l_D
SO	$\dfrac{C_1 q^3/l}{0.067\, q^3/l}$	$\dfrac{1}{\dfrac{1}{l_B}+\dfrac{1}{l_D}}$	$kz/(1+kz/l_0)$	$\alpha s_l \dfrac{\int qzdz}{\int qdz}$	1.0/15.0	$0.75+1.25\, z/z_i$; $z \le z_i$ or 2; $z > z_i$	$\left[2q^2 \Big/ \left(-R_1 \dfrac{\partial}{\partial z}\overline{\theta_{il}}\right)\right]^{1/2}$
AND	$\dfrac{\frac{C_1}{\sqrt{8}}\, q^3/l}{0.036\, q^3/l}$	$\mathrm{MIN}(l_B, l_D)$	$kz/(1+kz/l_0)$	$\alpha \dfrac{\int qzdz}{qdz}$	0.102	–	$0.75\left[\dfrac{q^2}{2} \Big/ \left(-R_1 \dfrac{\partial}{\partial z}\overline{\theta_{il}}\right)\right]^{1/2}$

Three types of turbulence time scales (τ, τ_θ, τ_3) have been discussed. These are defined by

$$\tau = \mu q^2/\bar{\varepsilon} \tag{34}$$

$$\tau_\theta = \mu\overline{\theta_{il}''^2}/\bar{\varepsilon}_\theta \tag{35}$$

$$\tau_3 = \tau/2.17\,. \tag{36}$$

From the earlier discussions about the parameterization of $\bar{\varepsilon}$, we can obtain τ by using Equation (34). Within the convective boundary, the ratio τ_θ/τ is about 0.5 as discussed by ZL. $\bar{\varepsilon}_\theta$ can be obtained from Equation (35). $\bar{\varepsilon}_r$ and $\bar{\varepsilon}_{\theta r}$ can be parameterized as

$$\bar{\varepsilon}_r = \frac{\overline{\mu r''^2}}{\tau_\theta} \tag{37}$$

$$\bar{\varepsilon}_{\theta r} = \frac{\mu\overline{\theta_{il}'' r''}}{\tau_\theta}\,. \tag{38}$$

3.5. The realization and the clipping approximation

In order to prevent the formation of nonphysical solutions to the turbulent flow, the enforced realizability for third-order moments as proposed by André *et al.* (1976) is used. We feel that it is also necessary to apply some constraints to the second-order moments. There is no proof that if third-order moments are constrained to be realizable, then the second moments will automatically be so.

The imperfect parameterization of the pressure covariances and dissipations can lead to the non-realizability of the second-order moments. Also, as mentioned before, ZL's scheme is sensitive to the turbulence time scale. We notice that an inappropriate parameterization of the turbulence time scale can cause non-realizability of second-order moments. The realization conditions for second and third-order moments are

(1) The variances are always greater than zero, i.e., $\overline{\alpha''^2} \geq 0$;

(2) The covariances are constrained by the products of the variances, $\overline{\alpha''\beta''} \leq (\overline{\alpha''^2}\,\overline{\beta''^2})^{1/2}$;

(3) The clipping approximation for the third-order moments (André *et al.* (1976)) is adopted, such that for a given third-order moment $\overline{\alpha''\beta''r''}$

$$|\overline{\alpha''\beta''\gamma''}| \leq \min \begin{cases} [\overline{\alpha''^2}(\overline{\beta''^2}\,\overline{\gamma''^2} + \overline{\beta''\gamma''}^2)]^{1/2} \\ [\overline{\beta''^2}(\overline{\alpha''^2}\,\overline{\gamma''^2} + \overline{\alpha''\gamma''}^2)]^{1/2} \\ [\overline{\gamma''^2}(\overline{\alpha''^2}\,\overline{\beta''^2} + \overline{\alpha''\beta''}^2)]^{1/2} \end{cases}$$

where α'', β'', and γ'' can be any fluctuating variable.

Boundary Conditions and the Initialization

A vertical staggered grid system similar to Cotton and Tripoli (1978) is used where the vertical grid increment Δz is 100 m. In this grid system, the variables $\bar{u}$, $\bar{v}$, $\overline{\theta_{il}}$, $\bar{r}$ and the third-order moments are co-located. All the second-order moments are located at intermediate or half-grid point levels. Figure 1 depicts the location of variables on the staggered grid. The spatial derivatives of the second-order moments are defined at the main levels and those of the third-order moments are defined at the intermediate levels.

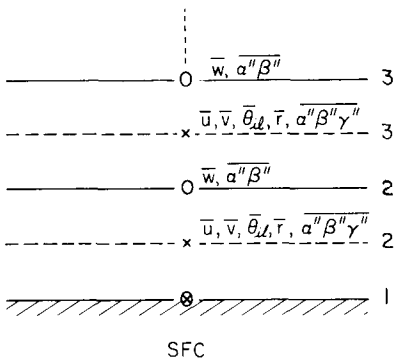

Fig. 1. Location of variables on the staggered grid. The dashed lines represent the main layers. The solid lines represent the intermediate layers.

There are 31 levels in the vertical and the time step for the integration is 2 s. The computer time needed for a 1-hour simulation is around 15 s. The time and space differencing scheme is the same as in the 3D core model (Cotton and Tripoli, 1978). Because the core model uses a time-split, non-hydrostatic solution to pressure, a smaller time step is employed for the acoustic wave, and a longer time step is used for the thermodynamic variables. In this 1D version of the higher-order turbulence model, mean gradients of pressure variations from the basic state are not evaluated. Therefore, a longer leapfrog time step is employed.

The initial conditions at 0900 LST, Day 33, Wangara, for θ_{il} and $\bar{r}$ are shown in Figures 2a, 3a. The large-scale geostrophic wind $\bar{u}_g$ is -5.5 m s^{-1} at the surface and varies linearly to -2.6 m s^{-1} at 1 km and to -1.2 m s^{-1} at 2 km (Wyngaard and Coté, 1974). The north–south geostrophic wind $\bar{v}_g$ is assumed to be zero. The initial $\bar{u}$ and $\bar{v}$ are similar to that shown in SO. The surface heat and moisture fluxes are based on the results of AND.

5. Results and Discussions

As indicated in Table I, two case studies based on a simplified version of AND and SO have been compared. To summarize the results, the AND case develops more TKE in the bulk of the boundary layer and has a faster growth rate of the boundary layer than the SO case.

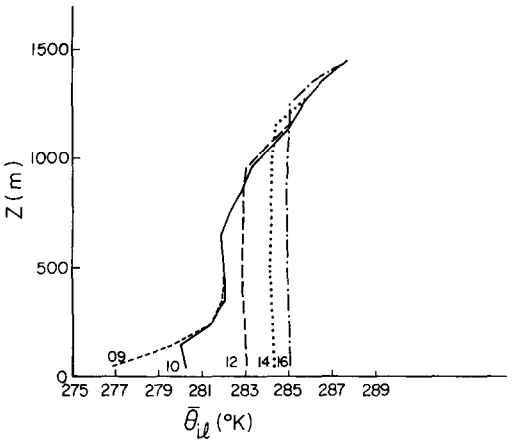

Fig. 2a. Computed profiles of the mean ice-liquid water potential temperature for the AND case during Day 33 of the Wangara Experiment.

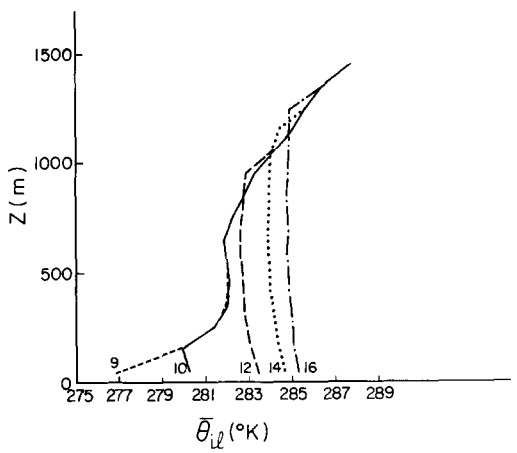

Fig. 2b. Same as Figure 2a, except for the SO case.

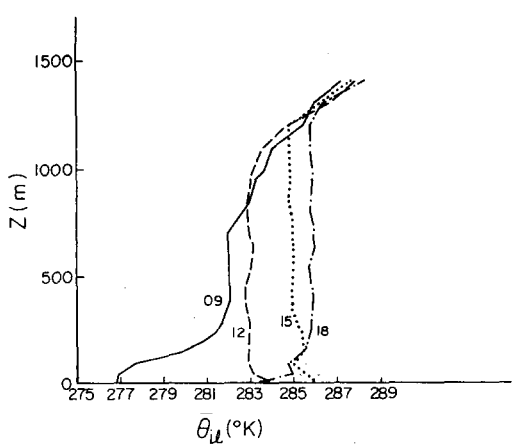

Fig. 2c. Observed profiles of the mean ice-liquid water potential temperature.

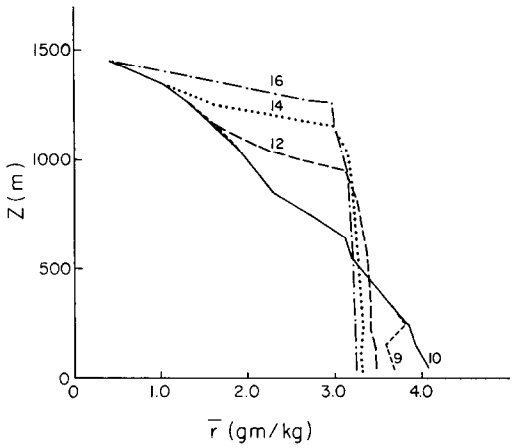

Fig. 3a. Computed profiles of the mean mixing ratio for the AND case during Day 33 of the Wangara Experiment.

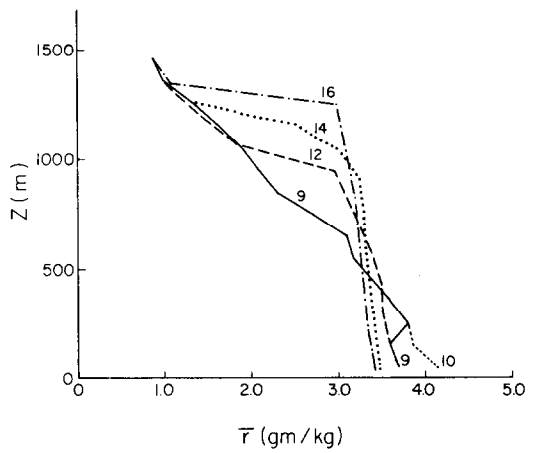

Fig. 3b. Same as Figure 3a, except for the SO case.

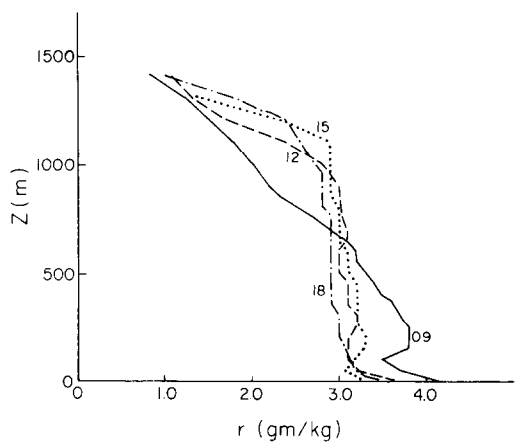

Fig. 3c. Observed profiles of the mean mixing ratio.

5.1. Evolution of mean variables ($\bar{\theta}_{il}$ and $\bar{r}$)

Figure 2a, b show computed evolutions of the mean ice-liquid water potential temperature profile ($\bar{\theta}_{il}$) for the AND and SO cases. Some features of these $\bar{\theta}_{il}$ profiles can be summarized as follows: (i) there is a shallow superadiabatic layer near the surface; (ii) this is followed by a deep and well mixed adiabatic layer; and iii) there is a well defined inversion at the top of the mixed layer. Figure 2c shows the observed evolution of the $\bar{\theta}_{il}$ profile. Comparing Figure 2a–c: (i) The AND case has a $0.1 \sim 0.2$ K higher $\bar{\theta}_{il}$ in the mixed layer than in the SO case; (ii) the AND case has a faster growth rate of the mixed-layer height between hours 12 and 14. The warmer temperature and faster growth rate of the mixed layer in the AND case can be attributed to a greater rate of entrainment at the top of the mixed layer. This is a consequence of greater turbulence kinetic energy in the AND case than the SO case. The reason for this difference can be traced to the larger turbulence time scale in the AND experiment; and (iii) after 15 h, the observed case has a warmer and shallower mixed layer. As discussed by Deardorff (1974), this may be attributed to large-scale subsiding vertical motion, which is not included in this paper.

Around noon, the AND case fits the observations best. At 12 h for example, the observed mixed layer has a depth of 1000 m, and the mean $\overline{\theta_{il}}$ within this layer is about 283 K. In the AND case, the mixed layer has a fast growth rate. The observed case shows a similar characteristic.

Figure 3a and 3b represent the computed evolution profile of the mean mixing ratio of the total water ($\bar{r}$) while Figure 3c shows the observed profile. Although for all three cases there is a slight and persistent decrease of $\bar{r}$ with respect to height, the total water seems to be well mixed in the adiabatic layer. As indicated by AND, this decrease of total water with height is attributed to the entrainment of dry air aloft during the rapid growth of the mixed layer. From Figure 3a and 3b, we find that the AND case produces a drier mixed layer than does the SO case. This can also be explained by a greater rate of entrainment at the top of the mixed layer. Therefore, the processes producing a warmer and drier mixed layer for the AND case are consistent with each other.

In Figure 3c, the observed case shows a much drier mixed layer between hours 12 to 18. This suggests that the observed case has greater entrainment than the modeled case. In addition, from hours 12 to 15 (Figure 3c), the total water mixing ratio does not decrease with respect to time in the lower part of the mixed layer. In Figure 3a and 3b this decrease of $\bar{r}$ with respect to time can be well defined from hours 10 to 16. Therefore, some other processes such as subsidence, advection or increased surface evapotranspiration are operating; these factors are not considered in the current simulation.

5.2. Second-order moments

Figure 4a and 4b represent the computed vertical heat flux ($\overline{w'' \theta_{il}''}$) for the AND and SO cases, respectively. Both cases exhibit a linear profile with respect to height throughout the depth of the mixed layer. A downward heat flux or entrainment can be found near the inversion layer. The magnitude of the downward heat flux is between

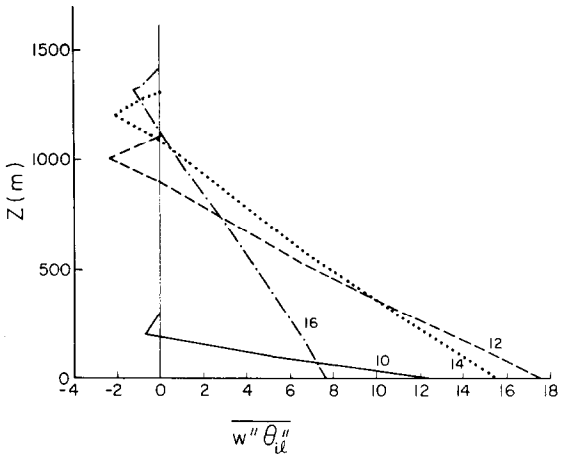

Fig. 4a. The computer profiles of the vertical heat flux $\overline{w'' \theta_{il}''}$ for the AND case.

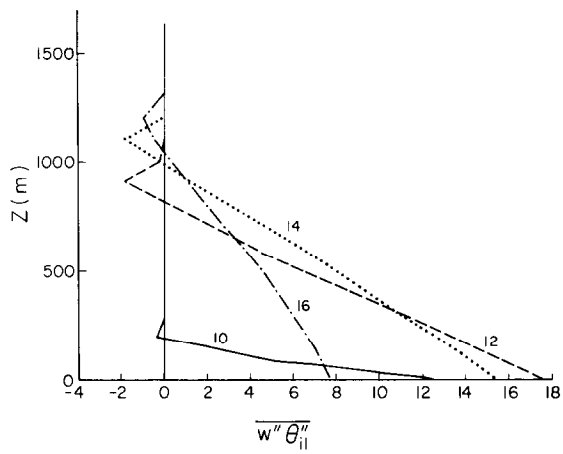

Fig. 4b. Same as Figure 4a, except for the SO case.

5 to 14% of its surface value. In general, the AND case has a larger downward heat flux at the top of the mixed layer than the SO case. This is a consequence of the larger magnitude of the vertical velocity variance ($\overline{w''^2}$) within the convective boundary layer (CBL) for the AND case. The downward heat flux at the top of the CBL is an indirect circulation which consumes energy. The energy is supplied from the middle or lower part of the CBL through the third-order moments. As noted by Brost *et al.* (1982), wind shear across the top of the mixed layer can also be a source of turbulent energy production for entrainment. The B term in Equation (2) represents the turbulent transport of energy by eddies which are dependent on $\overline{w''^2}$ within the CBL. Thus larger $\overline{w''^2}$ in the CBL can support larger downward heat flux at the top of the mixed layer.

Because the negative heat flux at the top of the mixed layer controls the entrainment rate and the growth rate of the mixed layer, a large downward heat flux implies a more rapid deepening of the mixed layer. This may explain the faster growth rate of the mixed layer height between hours 12 to 14 for the AND case.

Figure 5 shows the normalized profile of the vertical heat flux ($\overline{w'' \theta_{il}''}/w_* \theta_*$), where w_* and θ_* are the surface convective velocity and heat flux defined by $w_* = (g\overline{w'' \theta_{il}''} Z_I/\bar{\theta}_{il})_s^{1/3}$ and $\theta_* = (\overline{w'' \theta_{il}''})_s/w_*$, where the subscript s denotes surface and Z_I is the height of the inversion. In general, the AND case has larger negative slope of the heat flux profile $(\partial/\partial z)(\overline{w'' \theta_{il}''}/w_* \theta_*)$. This implies that the AND case has more vigorous mixing of $\bar{\theta}_{il}$ than the SO case.

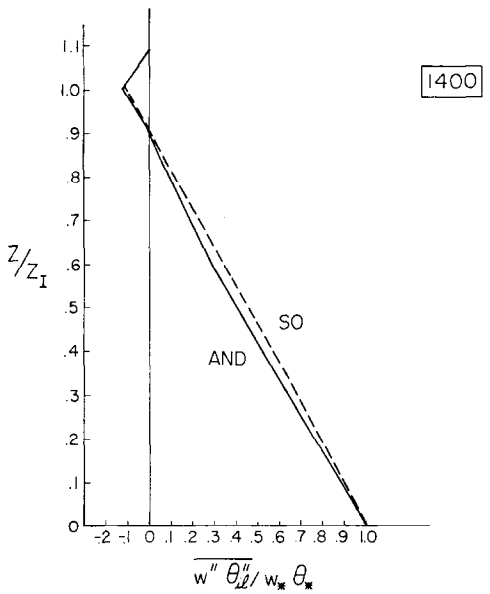

Fig. 5. The normalized profile of the vertical heat flux $\overline{w'' \theta_{il}''}/w_* \theta_*$.

The computed profiles of the vertical total water flux ($\overline{w'' r''}$) are shown in Figure 6a, b. The general increase of moisture flux with height in both cases is a consequence of entrainment of drier air from the layer above. The $\overline{w'' r''}$ profile for both cases shows a kink near the top of the mixed layer. The model results shown by Deardorff (1974) and André *et al.* (1978) exhibit a nearly smooth profile of $\overline{w'' r''}$. This kink of $\overline{w'' r''}$ can also be found in Sun and Ogura (1980). This may indicate that the kink is caused by the parameterization of the third-order term ($\overline{w''^2 r''}$).

The kink found in Figure 6a is an extreme case. The vertical profiles of $\overline{w''^2 r''}$ shown in Figure 13 indicate that the kink of $\overline{w'' r''}$ is directly related to the relatively larger $\overline{w''^2 r''}$ near the top of the mixed layer. The AND case even shows larger $\overline{w''^2 r''}$ than the SO case. From Figure 8 and Figure 13, we have learned that the third-order

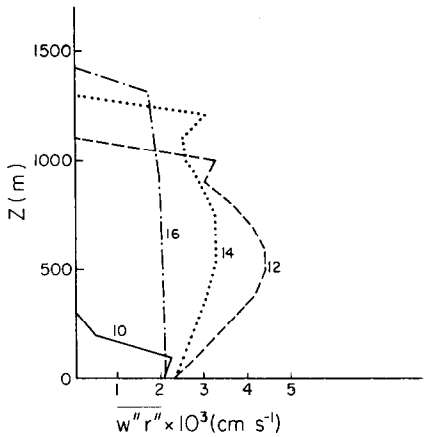

Fig. 6a. The computed profiles of the vertical total water flux $\overline{w''r''}$ for the AND case.

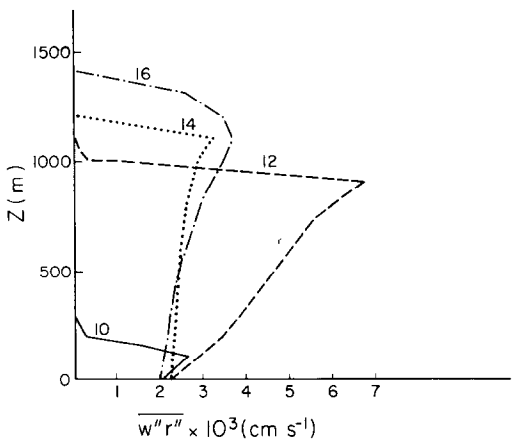

Fig. 6b. Same as Figure 6a, except for the SO case.

moments are sensitive to the magnitude of the turbulence time scale. This is the weakest aspect of ZL's type of parameterization for the third-order moments.

Figure 7 shows the normalized vertical velocity variance ($\overline{w''^2}/w_*^2$), which has a maximum located at $Z/Z_I = 0.25 \sim 0.3$ for the AND and SO cases. The AND velocity variance has a maximum value of 0.415 for $\overline{w''^2}/w_*$ while in the SO case, the maximum is about 0.32. As mentioned before, the larger entrainment rate or the larger downward heat flux at the top of the mixed layer for the AND case may be attributed to the larger vertical velocity variance produced in the convective boundary layer. Willis and Deardorff's (1974) laboratory experiment shows the normalized vertical velocity variance has a maximum of about 0.5 at $Z/Z_z = 0.4$. Therefore, the AND case is much closer to the laboratory experiment.

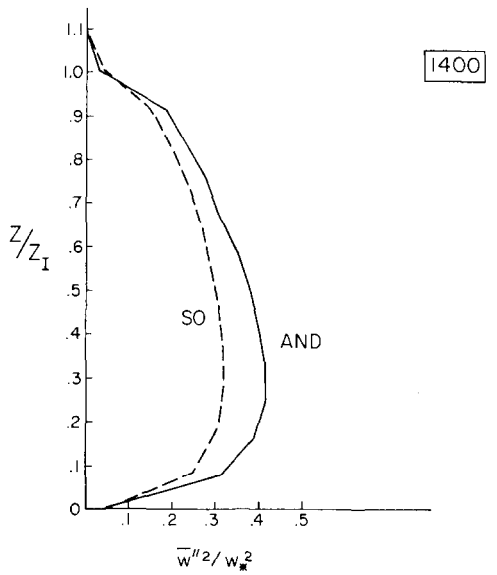

Fig. 7. The normalized vertical velocity variance. The dashed line represents the SO case, solid line is the AND case. The dashed-dot line indicates the case of Willis and Deardorff (1974).

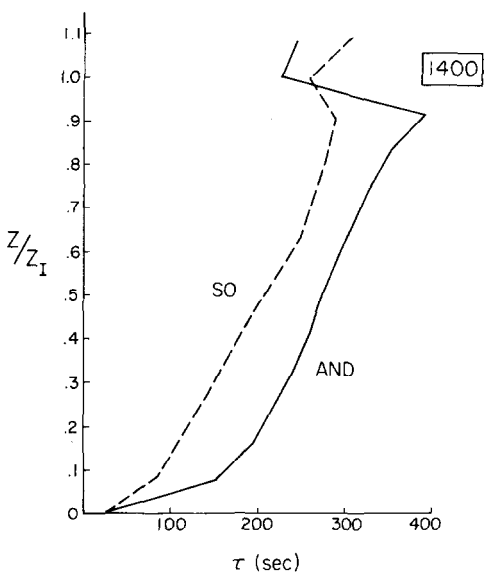

Fig. 8. The vertical profiles of the turbulence time scale. Solid line is for the AND case, dashed line is for the SO case. This result is at $t \approx 1400$ h.

Figure 8 shows the vertical profile of the turbulence time scale (τ) for the AND and the SO cases at 1400 LST. The major difference between the AND and SO cases is the magnitude of the turbulence time scale. The AND case has larger τ within most of the CBL. At the top of the mixed layer, the SO case has slightly larger τ. The parameter

S_l (see Table I) in the length scale parameterization of SO is the principal cause of the smaller τ within the CBL. The smaller turbulence time scale produces a larger rate of energy dissipation. This explains why SO has a smaller vertical velocity variance than does AND.

5.3. THE THIRD-ORDER MOMENTS

Figure 9 shows the vertical profile of the normalized $\overline{w''^3}$ which is responsible for the supply of turbulent kinetic energy to the top of the growing boundary layer. Within most of the CBL, the profile of $\overline{w''^3}$ is consistently greater in the AND case than in the SO case. This results in a greater transport of turbulent kinetic energy from the interior of the boundary layer to the inversion layer for the AND case. Because of the relatively larger magnitude of $\overline{w''^2}$ and $\overline{w''^3}$, the AND case may be considered a more 'active' convective boundary layer than the SO case. Both the AND and SO cases exhibit a negative $\overline{w''^3}$ near the surface which ZL have suggested is realistic. However, it is worthwhile to discuss the cause of this negative $\overline{w''^3}$. The only physical process that can cause it is down-gradient transport of $\overline{w''^2}$ (i.e., the term $-3\overline{w''^2}(\partial/\partial z)\overline{w''^2}$ in Equation 25). The buoyancy term contributes to positive production of $\overline{w''^3}$. Therefore, the negative value of $\overline{w''^3}$ near the surface may indicate an underestimation of the buoyancy contribution.

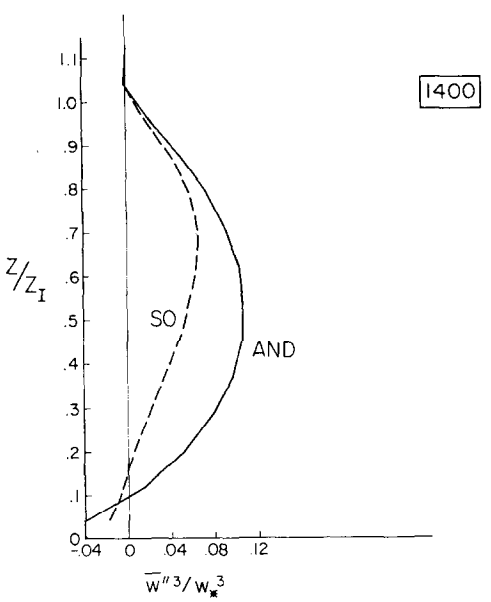

Fig. 9. Same as Figure 8, except for the normalized $\overline{w''^3}$ profile.

Figure 10 shows the normalized $\overline{w''\,\theta_{il}''^2}$ profile. Both AND and SO cases exhibit a relatively large positive flux near the surface and a small negative flux near the top of the mixed layer. From the sensitivity experiments, we have learned that there is no growth of the mixed layer whenever $\overline{w''\,\theta_{il}''^2}$ is negative near the surface. In order to

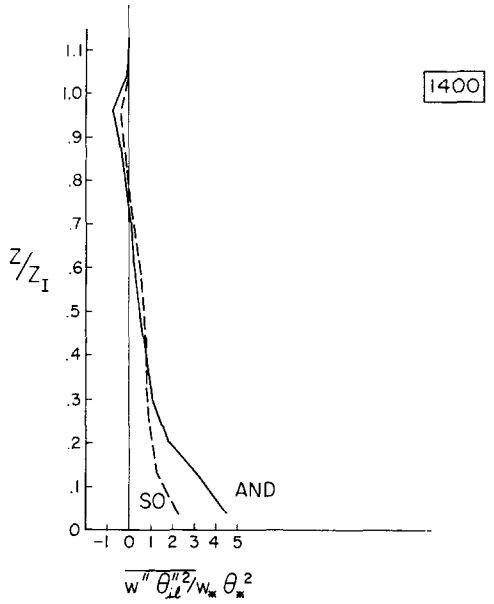

Fig. 10. Same as Figure 8, except for the normalized $\overline{w'' \theta_{il}''^2}$ profile.

obtain positive $\overline{w'' \theta_{il}''^2}$ near the surface, Zeman and Lumley (1976) and Sun and Ogura (1980) adjusted some parameters in their equations. Since our model contains an explicit parameterization of $\overline{\theta_{il}''^3}$, $\overline{\theta_{il}''^2 r''}$, $\overline{\theta_{il}'' r''^2}$, and $\overline{r''^3}$, such an adjustment was not necessary.

The largest differences between the AND and the SO cases can be seen in Figure 11.

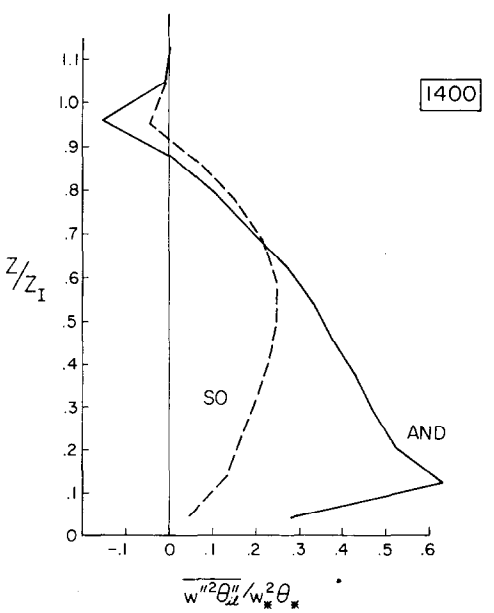

Fig. 11. Same as Figure 8, except for the normalized $\overline{w''^2 \theta_{il}''}$ profile.

The normalized profile of $\overline{w''^2\theta_{il}''}$ for the AND case exhibits a 'kink' near $Z = 0.12\ Z_I$. It is very difficult to decide which model result is most realistic. The observations reported by Telford and Warner (1964) support the AND case, while the results of Kaimal *et al.* (1976) agree with the SO case.

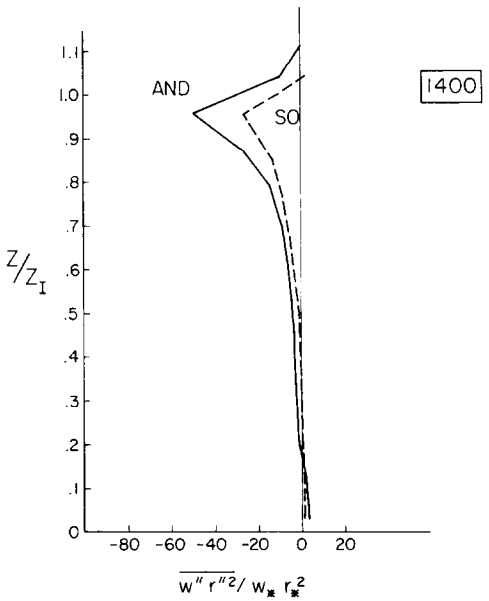

Fig. 12. Same as Figure 8, except for the normalized $\overline{w'' r''^2}$ profile.

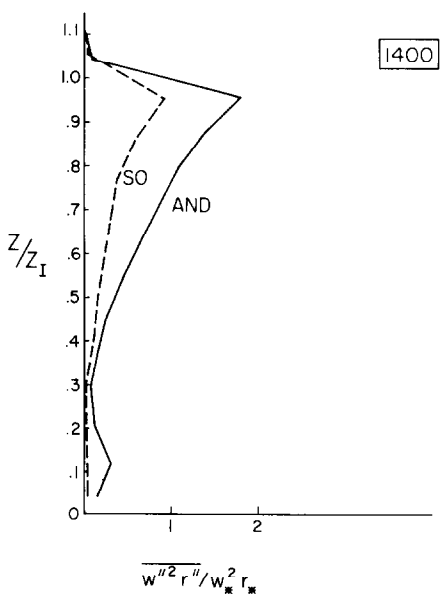

Fig. 13. Same as Figure 8, except for the normalized $\overline{w''^2 r''}$ profile.

Negative $\overline{w''^2\theta_{il}''}$ can be found near the top of the mixed layer for both cases. There are few data to verify the existence of this negative flux. The cause of negative $\overline{w''^2\theta_{il}''}$ is the term $-\overline{w''\theta_{il}''}(\partial/\partial z)\overline{w''^2}$ in Equation 28.

The profiles of $\overline{w''r''^2}$, $\overline{w''^2r''}$ for the AND and SO cases are shown in Figures 12 and 13. Both cases exhibit significant values of $\overline{w''r''^2}$ and $\overline{w''^2r''}$ in the upper part of the mixed layer. The vertical profile of $\overline{w''r''^2}$ reported by Lenschow and Wyngaard (1980) shows that the flux $\overline{w''r''^2}$ is positive throughout the entire mixed layer. The profile of $\overline{w''r''^2}$ shown in Figure 12 behaves differently from their results. We suspect that the cause of this discrepancy is the neglect of the term $(2\overline{w''^2r''}(\partial\bar{r}/\partial z))$ in ZL's parameterization for $\overline{w''r''^2}$ (see Equation (28)).

6. Summary and Conclusions

A partially-diagnosed second-order turbulence model has been described. The system is closed by the parameterization of the third-order moments following Zeman and Lumley (1976). All the equations are generalized to include total water and cloud water. A new scheme to parameterize the skewness terms is presented in order to satisfy realizability constraints. Different types of turbulence time-scale parameterization (André *et al.*, 1976; Sun and Ogura, 1980) are tested and compared. However, the AND case is not really the parameterization proposed by André *et al.* (1976). It is a simplified version, in which the effect of stable stratification on the numerical constant involved in dissipation parameterization is not taken into account. The major conclusions from this study are:

(1) The AND case produces a warmer and drier layer within the convective boundary layer.

(2) The SO case develops a smaller turbulence time scale within the bulk of the boundary layer.

(3) The AND case develops more vertical velocity variance over the bulk of the boundary layer.

(4) The AND case produces a larger entrainment rate.

(5) The Wangara observed data indicate that the large-scale vertical motion has significant impact on the evolution of the mixed layer in the afternoon.

(6) The sensitivity experiments reveal that ZL's parameterization of the third-order moments is sensitive to the turbulence time scale. To include the ratio l/l_B in the parameterization of dissipation is not appropriate, because this ratio will increase the turbulence time scale near the inversion. The main difference between SO and AND comes from the differing coefficients for q^3/l (shown in Table I) rather than from different length scales.

Based on these experiments, we shall adopt André *et al.*'s (1978) formulation of the length scale and dissipation in our stratocumulus model. The stratocumulus model described in the companion paper (Chen and Cotton, 1983) thus contains the following features:

(i) a one-dimensional version of the CSU cumulus model,

(ii) a partially-diagnostic second-order turbulence model,

(iii) Zeman and Lumley's (1976) parameterization for the third-order moments,

(iv) formulation of the length scale and parameterization of turbulence dissipation based on André *et al.* (1978).

Acknowledgements

The authors wish to thank Mr. Gregory J. Tripoli for his great help in setting up the model. Dr. Robert Banta is also acknowledged for his assistance in the development of the higher-order turbulence model. We also wish to thank Ms. Brenda Thompson for typing this very difficult manuscript. Ms. Judy Sorbie is also thanked for her excellent work in drafting the figures. This work was supported under Office of Naval Research Contract No. N00014–79–C–0793 and National Science Foundation Grant No. ATM–7908297. Computations were performed on the NCAR (National Center for Atmospheric Research) CRAY1 computer. NCAR is supported by the National Science Foundation.

References

André, J. C., DeMoor, G., Lacarrere, P., and DuVachat, R.: 1976, 'Turbulence Approximation for Inhomogeneous Flows', *J. Atmos. Sci.* **33**, 476–481.

André, J. C., DeMoor, G., Lacarrere, P., Therry, G., and DuVachat, R.: 1978, 'Modeling the 24-hour Evolution of the Mean and Turbulent Structures of the Planetary Boundary Layer', *J. Atmos. Sci.* **35**, 1861–1883.

Banda, R. and Cotton, W. R.: 1979, 'A Diagnostic Parameterization for Subgrid Covariances in a Boundary-Layer Model', Fourth Conference on Numerical Weather Prediction, Oct. 29–Nov. 1, 1979, pp. 360–363, Boston, AMS.

Blackadar, A. K.: 1962, 'The Vertical Distribution of Wind and Turbulent Exchange in Neutral Atmosphere', *J. Geophys. Res.* **67**, 3095–3102.

Brost, R. A., Wyngaard, J. C., and Lenschow, D. H.: 1982, 'Marine Stratocumulus Layers. Part II: Turbulence Budgets', *J. Atmos. Sci.* **39**, 818–836.

Chen, C. and Cotton, W. R.: 1983, 'A One-dimensional Simulation of the Stratocumulus-capped Mixed Layer', *Boundary-Layer Meteorol.* **25**, 289–321.

Cotton, W. R., and Tripoli, G. J.: 1978, 'Cumulus Convection in Shear Flow Three-dimensional Numerical Experiments', *J. Atmos. Sci.* **35**, 1503–1521.

Deardorff, J. W.: 1974, 'Three Dimensional Numerical Study of the Height and Mean Structure of a Heated Planetary Boundary Layer', *Boundary-Layer Meteorol.* **7**, 81–106.

Deardorff, J. W.: 1980, 'Stratocumulus-capped Mixed Layer Derived from a Three-dimensional Model', *Boundary-Layer Meteorol.* **18**, 495–527.

Kaimal, J. C., Wyngaard, J. C., Haugen, D. A., Coté, O. R., Tzumi, Y., Caughey, S. J., and Reading, C. J.: 1976, 'Turbulence Structure in the Convective Boundary Layer', *J. Atmos. Sci.* **33**, 2152–2169.

Lenschow, D. H., Wyngaard, J. C., and Pennell, W. T.: 1980, 'Mean Field and Second Moment Budget in a Baroclinic Convective Boundary Layer', *J. Atmos. Sci.* **37**, 1313–1326.

Manton, M. J. and Cotton, W. R.: 1977, 'Formulation of Approximate Equations for Modeling Moist Deep Convection on the Mesoscale', Atmospheric Science Paper No. 266, Colorado State University, 62 pp.

Moeng, C. H.: 1979, 'Stability of a Turbulent Layer Cloud Within the Planetary Boundary Layer', Ph.D. Thesis, The University of California, Los Angeles.

Oliver, D. A., Lewellen, W. S., and Williamson, G. G.: 1978, 'The Interaction Between Turbulent and Radiative Transport in the Development of Fog and Low-Level Stratus', *J. Atmos. Sci.* **35**, 301–316.

Sun, W.-Y. and Ogura, Y.: 1980, 'Modeling the Evolution of Convective Planetary Boundary Layer', *J. Atmos. Sci.* **37**, 1558–1572.

Telford, J. W. and Warner, J.: 1964, 'Fluxes of Heat and Vapor in the Lower Atmosphere Derived from Aircraft Observations', *J. Atmos. Sci.* **21**, 539–548.

Tripoli, G. J. and Cotton, W. R.: 1981, 'The Use of Ice-liquid Water Potential Temperature as a Thermodynamic Variable in Deep Atmospheric Models', *Mon. Wea. Rev.* **109**, 164–172.

Tripoli, G. J. and Cotton, W. R.: 1983, 'The Colorado State University Three-dimensional Cloud/Mesoscale Model – 1982', to be published in *J. de Rech. Atmos.*

Willis, G. E. and Deardorff, J. W.: 1974, 'A Laboratory Model of the Unstable Planetary Boundary Layer', *J. Atmos. Sci.* **31**, 1297–1307.

Wyngaard, J. C. and Coté, O. R.: 1974, 'The Evolution of a Convective Planetary Boundary Layer – A Higher-order Closure Model Study', *Boundary-Layer Meteorol.* **7**, 289–308.

Zeman, O. and Lumley, J.: 1976, 'Modeling Buoyancy Driven Mixed Layers', *J. Atmos. Sci.* **33**, 1974–1988.